Special Issue on "Medicinal Chemistry"

J. Indian Chem. Soc.,
Vol. 97, August 2020, pp. 1179-1189

Structure-based optimization of 2,3-dioxopyrrolidines as potential inhibitors of flaviviral methyltransferases

Prajakta Wangikar[a], Elvis A. F. Martis[a], Wahiba Aouadi[b], Santosh R. Nandan*[c], Etienne Decroly[b] and Evans C. Coutinho*[a]

[a]Molecular Simulations Group, Department of Pharmaceutical Chemistry, Bombay College of Pharmacy, Kalina, Santacruz East, Mumbai-400 098, India

[b]Aix-Marseille Univ, CNRS, AFMB UMR 7257, Marseille, France

[c]Ambernath Organics Pvt. Ltd., 222, The Summit Business Bay, Andheri (E), Mumbai-400 093, India

E-mail: evans.coutinho@bcp.edu.in, santosh.nandan@ambernathorganic.com

Manuscript received online 30 June 2020, accepted 20 July 2020

Various studies have shown that NS5 RNA methyltransferase (MTase) is a key enzyme involved in mRNA capping, a step crucial for flaviviral replication. Therefore, it has been identified as a potential target for therapeutic intervention in infections arising due to flaviviruses. In this paper, we report computer-assisted design of 2,3-dioxopyrrolidines, which were synthesised as guided by molecular docking studies on DENV and ZIKA MTase. Their chemical structures and geometric configuration were characterized by FT-IR, NMR (^{13}C and ^{1}H), MS and small molecule X-ray crystallography. Subsequently, their inhibitory potential was evaluated using an enzyme-based assay in DENV MTase (N7 and 2′O-MTase) and Zika virus MTase (N7 and 2′O-MTase). Furthermore, these molecules were also screened against RNMT (human N7 MTase). The most potent lead (compound **W07)** is seen to inhibit MTase from DENV with IC_{50} = 24.6±3.8 μM and ZIKA with IC_{50} = 9.0±1.7 μM. However, it also inhibits human N7 MTase, indicating plausible toxicity in humans. There is scope to further optimize these molecules to achieve selectivity towards flaviviral MTases.

Keywords: Flavivirus, methyltransferase, S-adenosyl-L-methionine, mRNA capping, 2,3-dioxopyrrolidines.

Introduction

Infections caused by flaviviruses pose a significant disease burden to many regions in the world. These include mosquito-borne Dengue (DENV), West Nile, Zika, Japanese encephalitis (JEV) and Yellow fever viruses which provoke life-threatening diseases with a devastating economic impact[1]. Despite the disease burden, there are no drugs or vaccines available for treating flaviviral infection except for JEV. The vaccine design faces many challenges owing to the presence of more than one viral serotype. Thus, incomplete protection against one serotype and secondary infection by any other serotype are associated with increased risk of developing severe infection. This process is referred to as antibody-mediated disease enhancement. Besides, there are several limitations, such as age and geographic differences, that discourage the use of currently designed vaccines[2,3]. The recently introduced live attenuated tetravalent vaccine 'Dengvaxia' (Sanofi Pasteur) is limited for age groups 9–45 years or 9–60 years (depending upon license) and is not recommended for children due to safety issues. Many countries that fall under dengue-endemic region have yet to register for this vaccine[4]. Moreover, the recent discovery of the fifth serotype of dengue virus (DENV5) may further limit the use of the tetravalent vaccine[5]. This scenario emphasises the necessity for developing antivirals against flaviviruses that can benefit the masses regardless of age and geographic area. The recent advancements in molecular biology of flaviviruses have highlighted the role of several proteins that are necessary for their replication. This has caught the attention of many researchers seeking to improve the therapeutic arsenal against flaviviral infections. In this vein, several targets are currently being investigated that are critical

for viral replication and growth, for example, the viral entry proteins, viral RNA polymerase/methyltransferase, nucleotide synthesis, viral helicase/NTPase, a viral serine protease, α-glucosidases and several kinases. Amongst these, NS5 RNA methyltransferase (MTase) is one vital target that has been thoroughly validated[6,7]. The MTase supports both N-7 and 2′-O methylation needed in the formation of type 1 cap (me7GpppA-me2) that is essential for mRNA stability and effective translation during infection[8–10]. This type 1 cap is generated through a four-step enzymatic reaction. In the first step, an RNA triphosphatase hydrolyses the 5′-triphosphate end of the nascent RNA to 5′-diphosphate. In the second step, RNA guanylyl transferase (GTPase) caps the 5′-diphosphate RNA with a GMP moiety from GTP. The third step involves the methylation at the N7 position using S-adenosyl-L-methionine (SAM) as a methyl donor. The last step is the methylation of the 2′-OH position of the first ribose nucleotide. This essential process of mRNA capping makes MTase an attractive target for antiviral drugs. Furthermore, it is observed that *flaviviruses* defective in N-7 methylation are non-replicative. Thus, inhibition of N-7 methylation has been shown to obstruct the viral replication, and therefore, making MTase a worthwhile target for antiviral interventions[7].

X-Ray crystallographic studies reveal that NS5 MTase possesses an overall globular fold that is divided into an N-terminal region, a core domain, and a C-terminal region[7,11]. The core domain possesses two specific binding sites, namely the SAM-binding site and the RNA binding site. This RNA-binding site is shallower and significantly solvent-exposed than the SAM-binding site[12]. Fig. 1 illustrates the SAM binding domain bound with the SAM analogs of the MTase from DENV and ZIKA.

In this paper, we report the design and synthesis of leads against DENV and ZIKA MTases. Using molecular docking, previously reported 2,3-dioxopyrrolidines[12] were optimized to improve their binding affinity for DENV and ZIKA MTases. A total of fifteen molecules were synthesized and characterized by FT-IR, ^{1}H and ^{13}C NMR and MS. Also, X-ray crystallographic studies were performed to confirm their geometry and configuration. All molecules were assayed for their activity against DENV and ZIKA MTase using enzyme-based assays. Further, the selectivity of these leads was measured by screening them against human MTases. The *in silico* ADME parameters were computed to understand their pharmacokinetic and safe toxicity profiles.

Materials and methods

Protein and ligand preparation:

The X-ray crystal structures of DENV3 MTase[13] (PDB id 3P8Z) and ZIKA MTase[14] (PDB id 5ULP) with inhibitors bound to the SAM-binding site were obtained from the Protein Data Bank. Using the protein preparation wizard in the Schrödinger

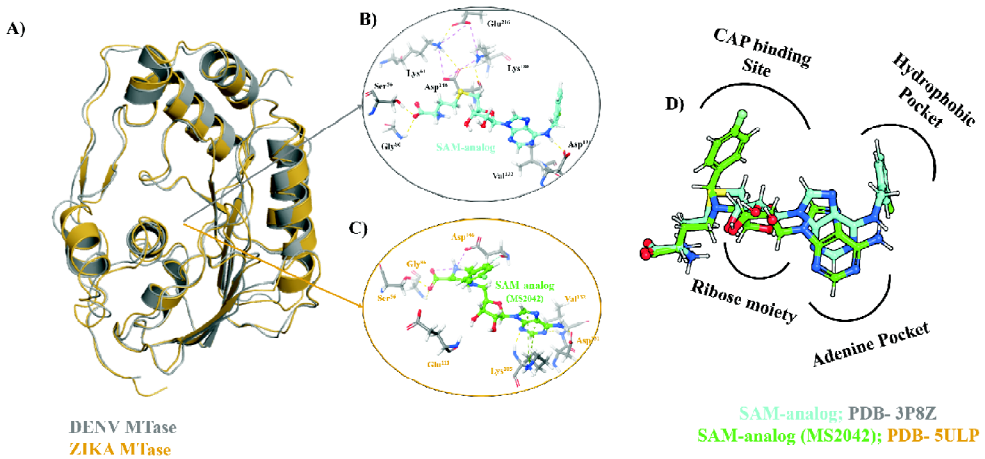

Fig. 1. **(A)** An overlay of X-ray crystal structures of DENV MTase and ZIKA MTase. **(B)** Protein-ligand interactions of DENV MTase and SAM-analog (PDB - 3P8Z; chain C). **(C)** Protein-ligand interactions of ZIKA MTase and SAM-analog-MS2042 (PDB - 5ULP). **(D)** Overlay of X-ray co-crystallised ligands bound to DENV MTase (Cyan sticks - SAM-analog) and ZIKA MTase (Green sticks - SAM-analog-MS2042). Yellow dotted lines indicate hydrogen bonds and magenta dotted lines indicate salt bridges.

modelling suite, the crystallographic water molecules beyond 5 Å from any inhibitor atom were deleted and hydrogen atoms were added to all heavy atoms. Later, atom types and partial charges were assigned by the OPLS2005 force field. The side-chain functional groups of acidic and basic amino acids were ionized corresponding to the physiological pH 7.4 using PROPKA[15] in the protein preparation wizard. Following the corrections made in the X-ray crystal structures, they were then minimized in vacuum for 5000 steps of steepest descents and 1000 steps of conjugate gradient using UCSF chimera[16]. To prepare the system for minimisation, the atom types for protein atoms and co-crystallized ligand atoms in the complex was assigned as per the AMBER14 (ff14SB) force field[17] and GAFF[18] (general amber force fields), respectively. Before docking, the geometries of the target molecules and co-crystallized ligands were optimized using the AM1 semiempirical method implemented in the semiempirical NDDO protocol using the BFGS optimizer in the Schrödinger suite.

Docking studies:

Molecular docking studies were performed using Autodock Vina[19]. The centre of mass of the co-crystallized ligands used to define the grid centre of the ligand box and the docking search space was extended to 20 Å and 25 Å in each direction for DENV3 and ZIKA MTase, respectively. The exhaustiveness parameter was set to 10. These parameters were finalized based on the results of re-docking of the co-crystallized ligand. All the necessary inputs files for docking with Autodock Vina were generated using MGLtools-1.5.6.

Computational ADME studies:

The ADME properties of the 2,3-dioxopyrrolidines were computed using *QikProp v3.3* in Schrödinger Suite, 2010. Some of the ADME properties that were computed using *QikProp* are given in Table S1 in the supplementary information. Donor HB (normal range 0.0–6.0) and Acceptor HB (normal range 2.0–20.0) represent the estimated number of hydrogen bonds that would be donated and accepted by the solute in an aqueous solution, respectively. The descriptor PSA i.e. polar surface area (normal range 7.0–200.0) describes the van der Waals surface area of polar nitrogen and oxygen atoms.

Chemical synthesis:

All solvents and reagents used for synthesis were of general reagent grade. All reactions were monitored by thin-layer chromatography (TLC) with Merck precoated silica plates (GF 254). Column chromatography was used to purify the final products. Melting points were recorded using a melting point apparatus and are uncorrected. All synthesized molecules were characterized by their spectral data (FT-IR/^{1}H and ^{13}C NMR/MS). Infra-red spectra were recorded on a Jasco FT-IR 5300 instrument (KBr disc method). NMR spectra (^{1}H and ^{13}C NMR) were recorded on a Bruker Avance-II model at 400 MHz. Chemical shifts are reported in ppm downfield from tetramethylsilane (TMS) as the internal standard. The coupling constants (*J*) are reported in Hertz (Hz). Mass spectra were recorded on an Agilent Technology 1260 Infinity LC equipped with an Agilent Technology 6120 Quadrupole mass spectrometer. The purity of compounds was confirmed by HPLC.

The synthetic pathway employed over here is principally a three-step procedure. In some cases, modification of the core (Fig. 2) after the third step was done to add diversity in the series. A total of fifteen derivatives of the core 4-alkylidene-2,3-dioxopyrrolidine were synthesized using different amines as the starting material and by incorporating various aromatic aldehydes in the third step of the synthesis. The compounds synthesized are grouped as Set A and Set B depending on the synthetic procedure as detailed below.

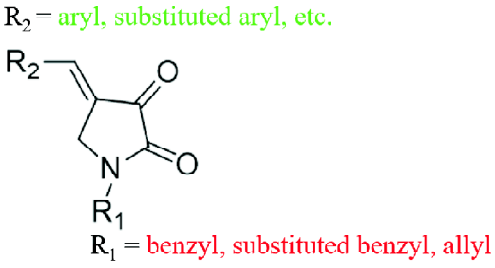

Fig. 2. Template/scaffold selected for synthesis.

General procedure for the synthesis of N-substituted 4-alkylidene-2,3-dioxopyrrolidine:

Equimolar quantities of amine (a) and ethyl acrylate (b) were dissolved in ethanol. After stirring overnight, the excess of solvent was distilled off when an oily product (c, the β-amino ester) separated. Equivalent amounts of diethyl oxalate (d) and sodium ethoxide in ethanol were then added to it. The reaction mixture was heated under reflux for several hrs and the excess solvent distilled off. The solid resi-

due was taken up in water and acidified with 20% HCl. The mixture was kept in a refrigerator overnight and the crystals which separated were filtered and dried to get the product (e)[20–22]. In the next step, compound (e) was decarboxylated and condensed with an aldehyde (f) by refluxing with 20% HCl (1 eq.) in a single combined approach to give the 4-alkylidene-2,3-dioxopyrrolidine (g). A total of thirteen molecules (**W01-W12, W15**) were synthesized with R_1 = benzyl, *p*-methoxybenzyl or allyl and R_2 = benzyl, substituted benzyl or naphthyl (Scheme 1, Table S2 in the Supplementary Information)[23,24].

General procedure for the synthesis of pyrrolo[3,4-b]pyridines from 1-benzyl-4-benzylidene-2,3-dioxopyrrolidin:

Equimolar quantities of 1-benzyl-4-benzylidene-2,3-dioxopyrrolidine and methyl β-aminocrotonate (methyl 3-aminobut-2-enoate) were dissolved in acetic acid. The reaction mixture was heated under reflux for 5–6 h and a sticky mass was obtained. The volatiles were removed under pressure. The product was washed with hexane and dried. The final compound (methyl 6-benzyl-2-methyl-7-oxo-4-phenyl-4,5,6,7-tetrahydro-1*H*-pyrrolo[3,4-*b*]pyridine-3-carboxylate, Scheme 2) was recrystallized from methanol[25,26].

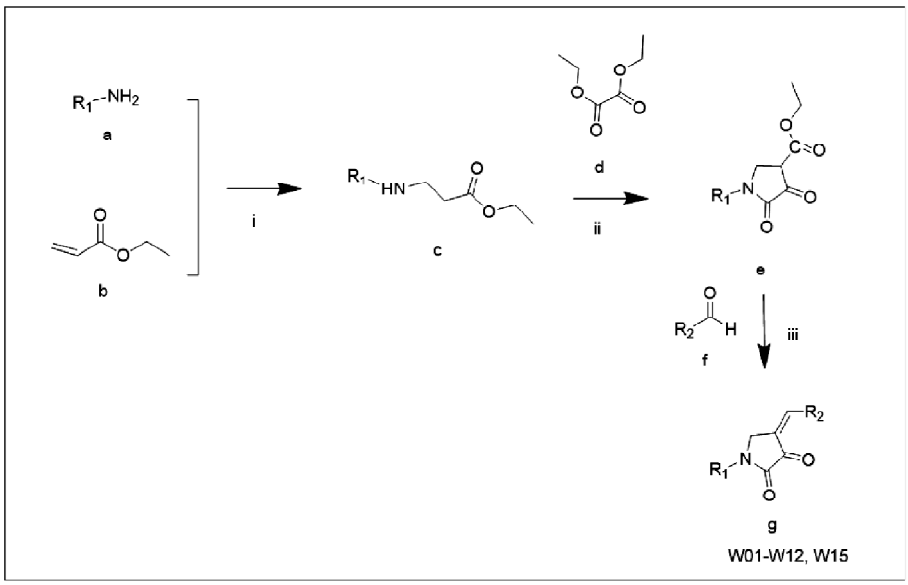

Scheme 1. Synthesis of *N*-substituted-4-alkylidene-2,3-dioxopyrrolidines (Reaction conditions: i – ethanol, stirring (24 h); ii – sodium ethoxide, ethanol, reflux (4–6 h); iii – reflux (8–12 h), methanol, 20% HCl).

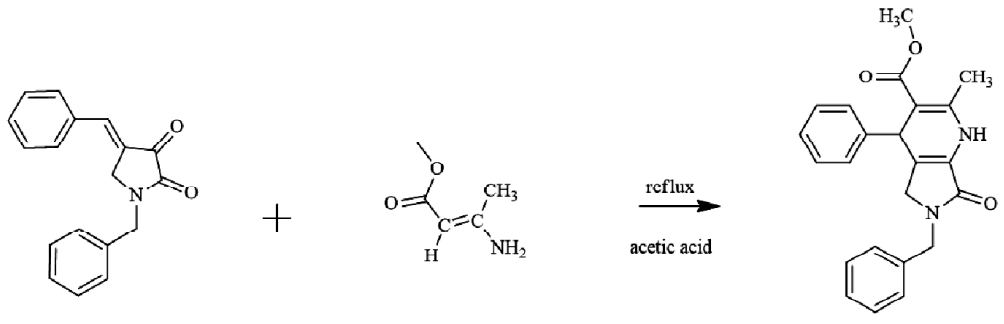

Scheme 2. Synthesis of pyrrolo[3,4-*b*]pyridines from benzylidene-2,3-dioxopyrrolidine (**W13**).

General procedure for the synthesis of pyrrolo[3,4-c]pyrazolone from 1-benzyl-4-benzylidene-2,3-dioxopyrrolidine:

The mixture of 4-benzylidene-2,3-dioxopyrrolidine (1 equiv) and hydrazine hydrate (1.5 equiv) were heated under reflux for 4–5 h in acetic acid. The reaction mixture was filtered and washed with water. The obtained solid was recrystallized from chloroform-hexane (2:1) (Scheme 3).

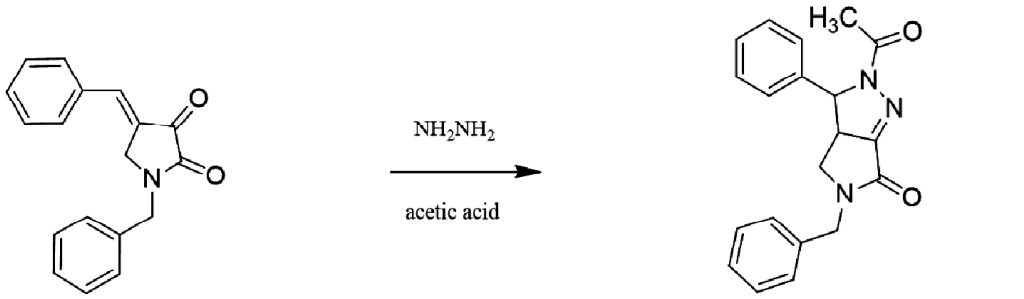

Scheme 3. Synthesis of 5-benzyl-3-phenyl-3,3*a*,4,5-tetrahydropyrrolo[3,4-*c*]pyrazol-6(2*H*)-one (**W16**).

Small molecule X-ray crystallography:

The detailed structural analysis by X-ray crystallography was performed for two molecules (**W01**, **W12**) to determine their geometry and configuration. Single crystals of these compounds were grown by slow evaporation of the solution of the compounds dissolved in solvents such as methanol or in a mixture of solvents like chloroform-hexane. The detailed procedure for data collection, reduction and refinement are given in the Supplementary Information.

Biological evaluation:

All compounds were evaluated for their inhibitory activity in DENV3 NS5 MTase (N7 and 2′O-MTase) and ZIKA Virus MTase. The enzyme-based assay was performed by measuring inhibition of radiolabeled [^{3}H]-SAM transfer onto synthetic capped RNA mimicking the viral mRNA 5′ end[27]. The compounds were dissolved in DMSO at 20 mM and diluted to 1 mM in 100% DMSO. The compounds were tested at a final concentration of 50 μM where SAH and sinefungin were used as control inhibitors and the substrate used was $GpppAC_4$ RNA. The enzymatic assays were performed in the presence of 5% DMSO. The MTase activity was followed by a filter binding assay using DEAE filters (dimethylaminoethanol)[28]. The DENV3 2′O-MTase assay (high concentration screening) was performed in 20 μL samples containing 40 mM Tris-HCl pH 7.5, 5 mM DTT, 10 μM AdoMet (0.2–2 μCi [^{3}H] AdoMet), 1 μM of DENV3 2′O MTase, 1 mM of compound (stock solutions 100 mM in 100% DMSO) and 1 μM $_{7Me}GpppAC_4$. The enzyme, buffer and compound were first mixed and the reaction was started with a premix of AdoMet and capped RNA substrates. Reactions were incubated at 30°C for 30 min and stopped by 20-fold dilution in an ice-cold 100 μM AdoHcy solution. Samples were then transferred onto a DEAE membrane (DEAE Filtermat; Wallace) by a Filtermat Harvester (Packard Instruments) washed with 0.01 *M* ammonium formate (pH 8.0), water and ethanol. Liquid scintillation fluid was added, and the radioactivity transferred onto RNA was measured using a Wallace 1450 MicroBeta Trilux Liquid Scintillation Counter. DENV3 N7-MTase activity was performed as described above but with 0.5 μM GpppA2′O^{Me}-RNA_{74} as the substrate. The counts per minute (c.p.m.) were detected in each experiment and the data was converted to % activity (100% of activity corresponds to the activity detected in the absence of any inhibitor)[29].

The MTase motif is also present in humans. Therefore, to understand specific inhibition, all compounds were tested against human N7 MTase. These enzymatic assays were performed as described above. The compounds exhibiting MTase inhibition were further tested with decreasing inhibitor concentration (with two-fold serial dilutions) to determine the inhibitor concentration at 50% activity (IC_{50}). The final

concentration of DMSO in reaction mixtures was below 5%. All data points were measured in duplicate. The IC_{50} values were determined using Prism software and adjusted to a logistic dose-response function: % activity = $100/(1 + [I]/IC_{50})^b$ where b corresponds to the slope factor and [I] to inhibitor concentration. All compounds were tested in duplicate at 50 μM (5% DMSO) concentration against DENV MTase (N7 and 2′O-MTase), RNMT (human N7 MTase) and ZIKA virus (N7 and 2′O-MTase)[30–32].

Results and discussion

2,3-Dioxopyrrolidines potentially mimics the SAM ribose moiety:

The docking validation was performed by redocking the co-crystallized ligands to their respective proteins. The current docking protocol was able to reproduce the X-ray bound conformation fairly well (heavy atom RMSD ~6 Å). We observe that both the co-crystallized ligands were quite flexible in nature, and therefore, a complete reproduction of the X-ray conformation was not attained. Nevertheless, the overall docked conformations were in general agreement with the binding conformation seen in the X-ray crystal structure as seen by the fact that the ribose and adenine rings superimposed very well (RMSD = 0.5 Å).

We embarked our investigation to find lead molecules against flaviviral methyltransferase by docking compound **9** (Fig. 3B) discovered by Podvinec *et al.*[12] by virtual screening, with a low micromolar inhibition of DENV MTase (IC_{50} = 4.4 μM). The compound **9** drew our attention and motivated us to explore it further because of the presence of the 2,3-dioxopyrrolidine ring. This ring can potentially biosterically mimic the ribose ring present in S-adenosylmethionine which is the methyl donor central to the RNA capping chemistry. Our docking studies indicate that the 2,3-dioxopyrrolidine ring superimposes quite well with the ribose moiety of SAM-analog (Fig. 3A). It is well established that SAM and the SAM-analog (Fig. 3A), the latter being an inhibitor, share identical binding conformations[13], and therefore, we deduce that the 2,3-dioxopyrrolidine occupies the same site as the ribose ring. The X-ray crystallographic analysis suggests that the ribose ring interacts with Glu111 through water-mediated hydrogen bonds[13]. Our docking analysis also shows that the 2,3-dioxopyrrolidine oxygen of compound **9** retains this water-mediated hydrogen bonds with Glu111 backbone oxygen. Additionally, it also shows water-mediated hydrogen bonds with the backbone NH of Gly106 and the side chain OH group of Thr104. Furthermore, the benzylmethoxy group of compound **9** is held steady in the adenine binding pocket of SAM (Figs. 1D and 3A) by two polar interactions. First is the cation-π interaction between the benzyl ring and the NH_3^+ group in the Lys105 side chain, and the second is a hydrogen bond between the methoxy oxygen and the backbone NH of Phe133. Moreover, the carboxylate group that we anticipated would mimic the carboxylic group in the amino acid side chain of SAM, binds rather loosely, since the carbon chain length of compound **9** is two carbons too short to extend and overlap with carboxylate group of SAM. Owing to this, a few polar interactions are lost, and we propose that this is the primary reason for the lower affinity of compound **9** compared with the SAM-analog (K_i = 0.24 μM). The SAM-analog was found to extend its N7 benzyl ring into the hydrophobic pocket[13] (Figs. 1D and 3A) through which it attains highly selective inhibition of DENV MTase and not against human N7 MTase, which lacks this hydrophobic pocket.

Having identified the binding conformation of compound **9**, we made modifications to strengthen the interactions in the adenine pocket and to reach the hydrophobic pocket. During the computational lead design studies we predicted that replacing the benzylmethoxy group of compound **9** with a naphthyl ring and replacing the propionic acid group with a benzyl group leading to compound **W07** would provide significant rigidity to the molecule while retaining crucial interactions of the 2,3-dioxopyrrolidine to mimic the ribose interactions of SAM and SAM-analog. The docking-based predictions show that the 2,3-dioxopyrrolidine oxygen of compound **W07** shows a direct hydrogen bond with the side-chain NH of His110, and therefore, holds the 2,3-dioxopyrrolidine ring close to the ribose binding region of SAM. Furthermore, as we replace the methoxy group of compound **9** with a completely non-polar naphthyl ring in compound **W07**, the hydrogen bond with the backbone NH of Phe133 is lost and is replaced with an aromatic hydrogen bond[33] with the side-chain carboxylate group of Asp131. The naphthyl ring was able to retain the cation-π interaction with NH_3^+ in the Lys105 sidechain (Fig. 3C).

The ZIKA MTase shares good amino acid identity with very high fold similarity to DENV MTase (backbone RMSD < 1 Å). Therefore, we found it worthwhile to investigate whether compound **W07** shows any affinity towards ZIKA MTase. The

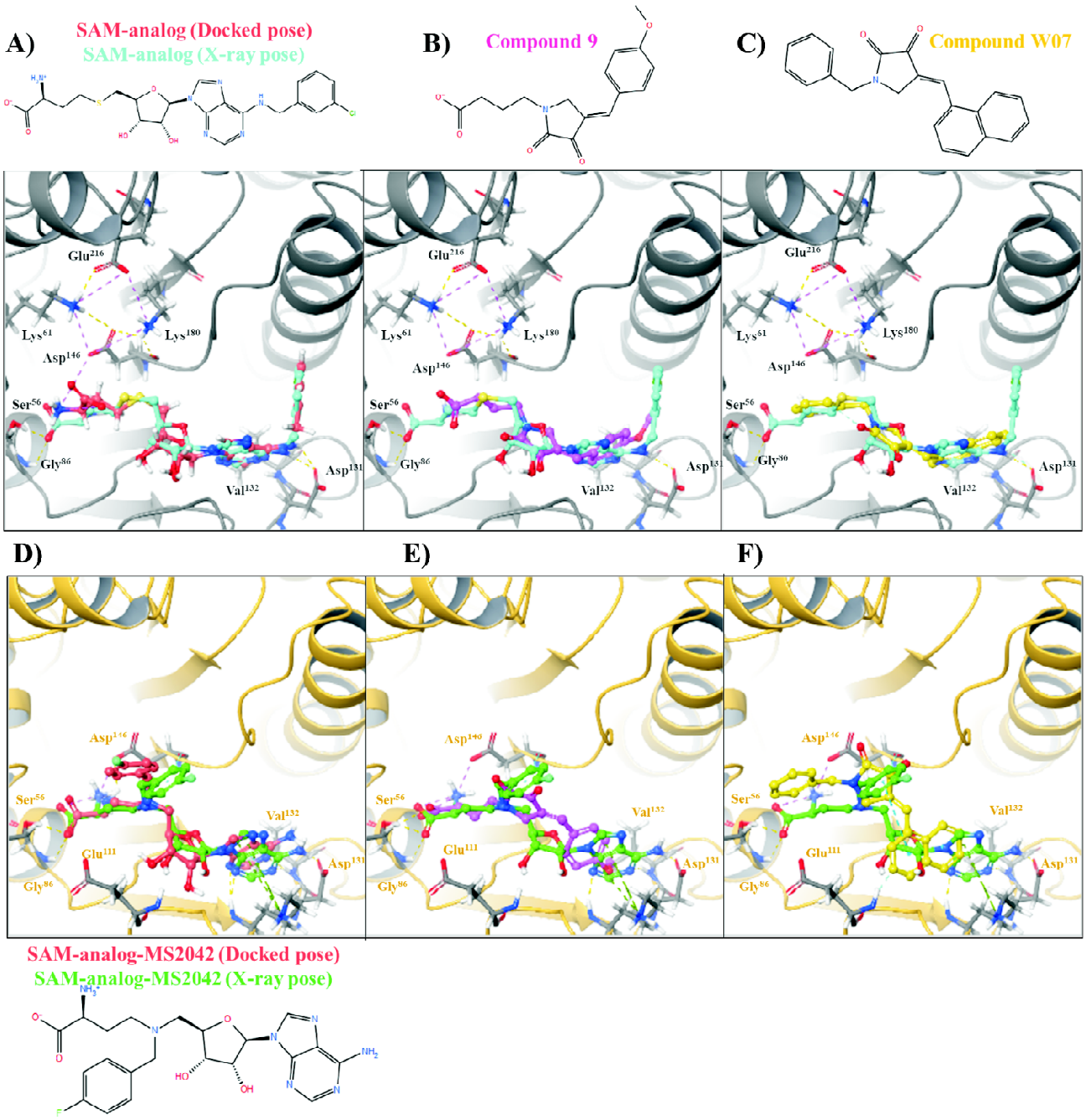

Fig. 3. **(A)** Docking validation for DENV MTase by redocking SAM-analog. **(B)** Protein-ligand interactions obtained by docking of compound **9** in DENV MTase catalytic site. **(C)** Protein-ligand interactions obtained by docking of compound **W07** in DENV MTase catalytic site. **(D)** Docking validation for ZIKA MTase by redocking SAM-analog (MS2042). **(E)** Protein-ligand interactions obtained by docking of compound **9** in ZIKA MTase catalytic site. **(F)** Protein-ligand interactions obtained by docking of compound **W07** in ZIKA MTase catalytic site. Yellow dotted lines indicate hydrogen bonds and magenta dotted lines indicate salt bridges.

docking exercise was repeated for the compounds **9** and **W07**. Our docking predictions suggested that, despite the great similarity between the two MTases, the 2,3-dioxopyrrolidine ring might not bind akin to the ribose ring. In this case, the 2,3-dioxopyrrolidine ring was found approaching the cap binding site (Figs. 1D, 3C and 3F), however it

retains the cation-π interaction with NH_3^+ in the Lys105 sidechain of ZIKA MTase. Further, compound **9** was able to extend its carboxylate group and mimic the polar interactions of SAM-analog (MS2042) with Ser56 (which is conserved residue in DENV3 MTase). As the compound **W07** lacks a polar group, this interaction was lost. The biological assays corroborate our docking predictions by suggesting that the compound **W07** is the most potent molecule in this series, however, it lacks selectivity as it was found to bind MTase from human (*vide infra*).

Small molecule X-ray crystallographic analysis:

N-Substituted-4-alkylidene-2,3-dioxopyrrolidines can exist as *E* or *Z* isomers due to the presence of the olefinic bond connecting the phenyl group to the pyrrolidine ring. Since it is a tri-substituted double bond, isomer analysis by ^{1}H NMR is difficult without a reference standard. Hence, X-ray crystallographic studies were performed on two different molecules to confirm their structures[34,35] (Fig. 4). X-Ray crystallography analysis unravelled many structural aspects that were difficult to resolve using NMR or other spectroscopic techniques. The overall structures of both molecules are similar with slight differences in the torsions and bond angles. The crystals of molecule **W01** belong to the primitive triclinic cell with dimensions a = 6.410(1) Å, b = 7.465(2) Å, c =15.274(3) Å, V = 711.9(2) Å^3, Z = 2 and Dc = 1.294 g/cm^3. The ORTEP diagram of **W01** (Fig. 4A) shows that the phenyl (**A1**) and pyrrolidine rings form an overall extended structure except for the torsion angle N1-C5-C6-C7 (–105.48°) which indicates folding of the other aromatic ring (**A2**) in a gauche arrangement. The crystals of molecule **W12** (Fig. 4B) belong to the primitive monoclinic cell with dimensions a = 10.2749(5) Å, b = 14.9137(8) Å, c = 11.2833(5) Å, V = 1616.59(2) Å^3, Z = 4 and Dc = 1.328 g/cm^3. Here also, the phenyl (**A1**) and pyrrolidine ring form a planar structure whereas the other aromatic ring (**A2**) lies in a different plane with the torsion angle N1-C12-C18-C13 (–118.70°) rendering a gauche arrangement. A unique feature is seen in case of molecule **W12**, with two intermolecular H-bonds. The first is between the carbonyl oxygen (O3) of molecule A with the hydroxyl group (O1-H1) of molecule B (hydrogen bond distance O1-H1(5)···O3(1) = 3.449 Å); and the second is between hydroxyl group (O1-H1) of molecule A with the carbonyl oxygen (O3) of molecule C (hydrogen bond distance O1-H1(1)···O3(3) = 3.449 Å) (Supplementary Fig. S2A). The network of intermolecular hydrogen bonds gives the molecule a helical arrangement (Supplementary Fig. S2B). The crystallographic data also reveals that the molecules exist as *E* isomers at the olefinic bond connecting the pyrrolidine ring to the phenyl group (**A1**) i.e. the phenyl ring (**A1**) and the keto group of pyrrolidine ring are on opposite sides of the double bond[36].

2,3-Dioxopyrrolidines inhibit a wide range of MTases:

Sinefungin and SAH (SAM by-product) were found to completely inhibit all the MTases considered in this work at

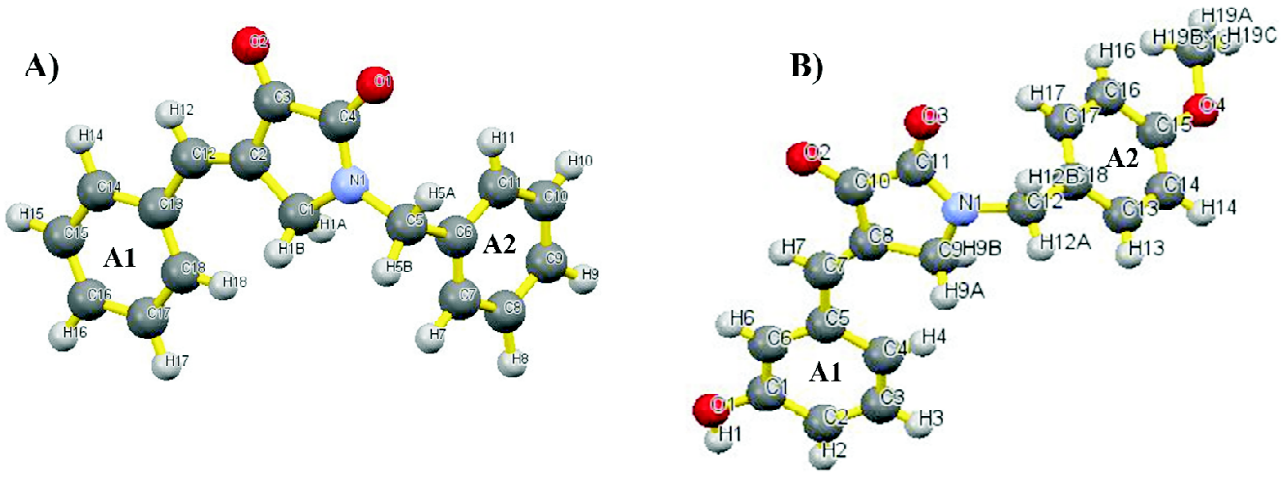

Fig. 4. An ORTEP diagram (with atom numbering scheme) of molecule **(A)** W01 and **(B)** W12.

50 µM which were used a positive controls alongwith DMSO as the vehicle control, which does not inhibit any of the MTases. The assays show that all MTases are more susceptible to senifungin than SAH (Fig. S1 in the Supplementary Information**)**. Our compounds **W04**, **W05**, **W06**, **W07**, **W09** and **W11** exhibit more than 40% inhibition against DENV MTase (N7 and 2′O-MTase), RNMT (human N7 MTase), and ZIKA virus (N7 and 2′O-MTase) assays. Interestingly, the compound **W03** shows 40% inhibition only against human N7 MTase and ZIKA virus (N7 and 2′O-MTase). Further, the compounds **W01**, **W02**, **W08**, **W10**, **W12**, **W13**, and **W15** show 40% of human N7 MTase and fail to show any significant inhibition of other MTases. The order of activity of the compounds (Fig. 5A) was found to be **W07** > **W06** > **W09** > **W04** > **W05**. No significant inhibition was detected for the other compounds in the DENV MTase assay.

The IC_{50} was determined for compounds that showed good inhibition of ZIKA virus MTase (Fig. 6B), and RNMT (human N7 MTase) (Fig. 6C). The compounds **W01**, **W03**, **W04**, **W05**, **W06**, **W07**, **W09**, and **W11** also inhibit ZIKA virus MTase. The order of activity of the compounds was found to be **W07** > **W05** > **W06** > **W04** > **W09** > **W03** > **W01** > **W11**. It is evident from the results that compound **W07** also inhibits ZIKA virus MTase (IC_{50} = 9.0±1.7 µM) (Fig. 5B). Nevertheless, all the above-mentioned compounds inhibit human N7 MTase at lower IC_{50} (Fig. 5C). Thus, the compounds are non-selective inhibitors of MTase and need more structural manipulations to gain selectivity.

Our design strategy started with modifying a previously reported hit (compound **9**)[12] by replacing a benzylmethoxy group, that occupies the adenine pocket, with a naphthyl group and the propionic acid group with a benzyl moiety. This initial modification led us to the most potent molecule in these series (compound **W07**). However, the compound **W07** was found to be a non-selective inhibitor of all the Mtases used in this study. Therefore, to improve the inhibition and attain selectivity, we replaced the naphthyl ring with 3-nitrobenzyl group leading to compound **W06**. This modification led to a 2-fold drop in the activity across all MTases including the human MTase. Our docking predictions suggest

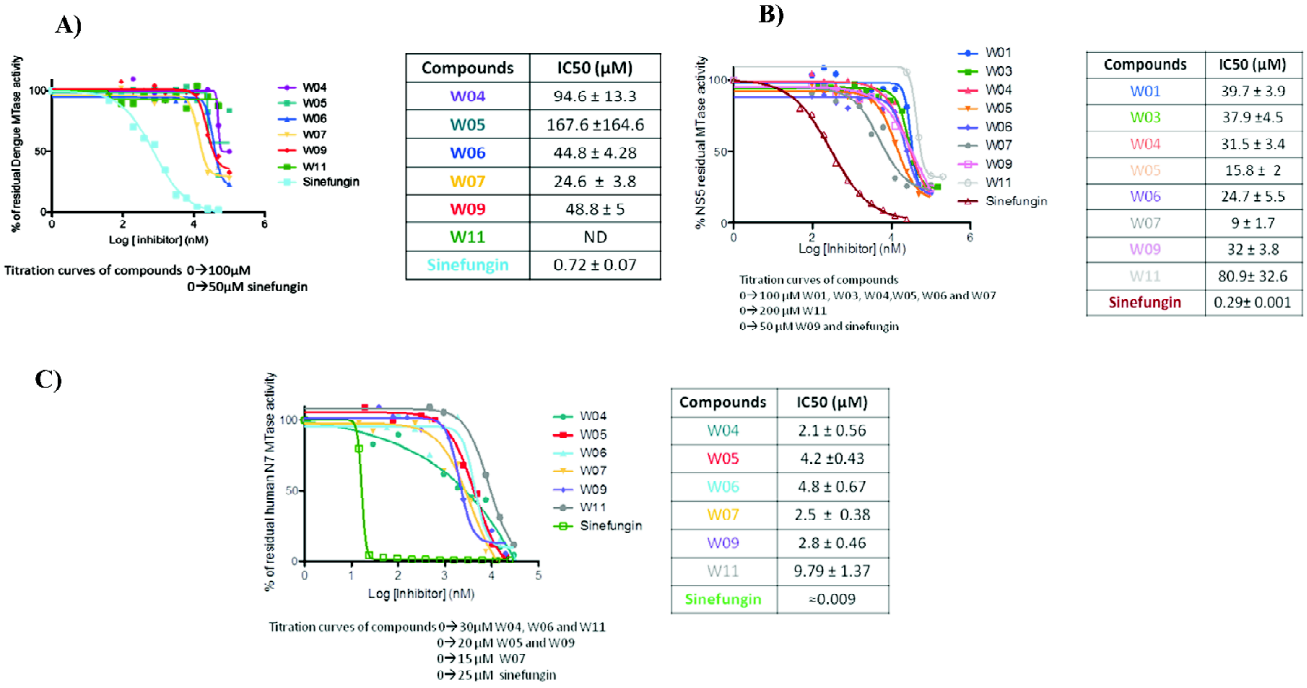

Fig. 5. Results of the bioassay against various MTases. **(A)** DENV MTase, **(B)** ZIKA Viral MTase and **(C)** Human N7 MTase.

that the drop in the activity of **W06** is the loss of crucial aromatic hydrogen bonds due to replacement of the naphthyl ring. Since compound **W06** showed a drop in the activity of human MTase, we further modified it by adding a 4-fluoro group leading to compound **W05**. We observed that the compound **W05** showed a 4-fold drop in the activity against DENV MTase. In this case, our docking simulation was unable to explain such a large drop in DENV MTase activity owing to a small change in the structure. Interestingly, a moderate improvement of activity was seen against ZIKA and human MTases. Any further modifications, either completely abolished the activity or improved its activity against human MTase leading to more non-selective molecules.

Conclusions

The object of this study was to optimise 2,3-dioxopyrrolidines against flaviviral MTase. We employed molecular docking-based predictions to guide substitutions with improved binding. The structures predicted by docking were synthesized and tested by direct enzyme-based assays on MTases from DENV, ZIKA, and human. During, this exploration the compound **W07** was found to be the most potent in the series. It also shows good inhibitory potential against other MTases indicating non-selective inhibition. Therefore, certain modifications are required to achieve selective inhibition of DENV and ZIKA MTase. Since the molecular weights of all lead molecules studied here are in the range 227–340 there is scope for further optimisation to improve activity and selectivity. Our findings have disclosed strategies that can be explored to achieve inhibition against flaviviral MTase (DENV and ZIKA). Therefore, we conclude that developing flavivial MTase inhibitors is still a challenging task, besieged with selectivity issues due to the overabundance of MTase in the host cell. However, the significance of this enzyme in the viral replication process cannot be underrated. Hence, flavivirus MTase remains an attractive target for antiviral development.

Acknowledgements

The authors are grateful to the Lady Tata Memorial Trust for funding this project, AFMB University of France for providing the facility of enzyme assay, SAIF Punjab University (Chandigarh) for the NMR studies, Center of Excellence (Rajkot) for X-ray crystallography, Ambernath Organics (Mumbai) for LCMS and MKR Laboratories (Mumbai) for providing us with analytical services.

Supporting Information

Supplementary Information submitted as separate documents.

References

1. R. Qi, L. Zhang and C. Chi, *Acta Biochim. Biophys. Sin.*, 2008, **40(2)**, 91.
2. D. J. Gubler, *Clin. Microbiol. Rev.*, 1998, **11(3)**, 480.
3. M. Bollati, K. Alvarez, R. Assenberg, C. Baronti, B. Canard, S. Cook, *et al., Antiviral Res.*, 2010, **87(2)**, 125.
4. World Health Organization. Dengue vaccine: WHO position paper-July 2016, Weekly Epidemiol Rec., 2016, **91(30)**, 349.
5. M. Mustafa, V. Rasotgi, S. Jain and V. Gupta, *Med. J. Armed Forces India*, 2015, **71(1)**, 67.
6. A. Sampath and R. Padmanabhan, *Antiviral Res.*, 2009, **81(1)**, 6.
7. H. Dong, B. Zhang and P.-Y. Shi, *Antiviral Res.*, 2008, **80(1)**, 1.
8. K. Y. Chung, H. Dong, A. T. Chao, P.-Y. Shi, J. Lescar and S. P. Lim, *Virology*, 2010, **402(1)**, 52.
9. C. G. Noble, S.-H. Li, H. Dong, S. H. Chew and P.-Y. Shi, *Antiviral Res.*, 2014, **111**, 78.
10. E. Decroly, F. Ferron, J. Lescar and B. Canard, *Nat. Rev. Microbiol.*, 2012, **10(1)**, 51.
11. C. Bussetta and K. H. Choi, *Biochemistry*, 2012, **51(30)**, 5921.
12. M. Podvinec, S. P. Lim, T. Schmidt, M. Scarsi, D. Wen and L.-S. Sonntag, *et al., J. Med. Chem.*, 2010, **53(4)**, 1483.
13. S. P. Lim, L. S. Sonntag, C. Noble, S. H. Nilar, R. H. Ng, G. Zou, *et al., J. Biol. Chem.*, 2011, **286(8)**, 6233.
14. R. Jain, K. V. Butler, J. Coloma, J. Jin and A. K. Aggarwal, *Sci. Rep.*, 2017, **7(1)**, 1.
15. M. Rostkowski, M. H. Olsson, C. R. Søndergaard and J. H. Jensen, *BMC Struct. Biol.*, 2011, **11(1)**, 1.
16. E. F. Pettersen, T. D. Goddard, C. C. Huang, G. S. Couch, D. M. Greenblatt, E. C. Meng, *et al., J. Comput. Chem.*, 2004, **25(13)**, 1605.
17. J. A. Maier, C. Martinez, K. Kasavajhala, L. Wickstrom, K. E. Hauser and C. Simmerling, *J. Chem. Theory. Comput.*, 2015, **11(8)**, 3696.
18. J. Wang, R. M. Wolf, J. W. Caldwell, P. A. Kollman and D. A. Case, *J. Comput. Chem.*, 2004, **25(9)**, 1157.
19. O. Trott and A. J. Olson, *J. Comput. Chem.*, 2010, **31(2)**, 455.

20. P. L. Southwick and R. T. Crouch, *J. Am. Chem. Soc*., 1953, **75(14)**, 3413.
21. G. Stork and S. McElvain, *J. Am. Chem. Soc*., 1947, **69(4)**, 971.
22. P. L. Southwick, E. P. Previc, J. Casanova (Jr.) and E. H. Carlson, *J. Org. Chem*., 1956, **21(10)**, 1087.
23. P. L. Southwick and E. F. Barnas, *J. Org. Chem*., 1962, **27(1)**, 98.
24. P. L. Southwick, N. Latif, B. M. Fitzgerald and N. M. Zaczek, *J. Org. Chem*., 1966, **31(1)**, 1.
25. Y. Sato, Y. Shimoji, H. Fujita, H. Mizuno and S. Kumakura, *Yakugaku Zasshi*., 1978, **98(4)**, 448.
26. P. Devasthale, W. Wang, L. G. Hamann and J. M. Fevig, US Patents (US 7,521,557 B2), 2009 April 21.
27. M.-P. Egloff, E. Decroly, H. Malet, B, Selisko, D. Benarroch, F. Ferron, *et al., J. Mol. Biol*., 2007, **372(3)**, 723.
28. B. Coutard, E. Decroly, C. Li, A. Sharff, J. Lescar, G. Bricogne, *et al., Antiviral Res*., 2014, **106**, 61.
29. K. Barral, C. Sallamand, C. Petzold, B. Coutard, A. Collet, Y. Thillier, *et al., Antiviral Res.*, 2013, **99(3)**, 292.
30. F. Peyrane, B. Selisko, E. Decroly, J.-J. Vasseur, D. Benarroch, B. Canard, *et al., Nucleic Acids Res*., 2007, **35(4)**, e26.
31. W. Aouadi, A. Blanjoie, J.-J. Vasseur, F. Debart, B. Canard and E. Decroly, *J. Virol*., 2016, **JVI.02217-16**.
32. A. DeLean, P. Munson, D. Rodbard, *Am. J. Physiol-Endocrinol Metab*., 1978, **235(2)**, E97.
33. M. Levitt and M. F. Perutz, *J. Mol. Biol.*, 1988, **201(4)**, 751.
34. J. Pflugrath, *Acta Crystallogr. D: Biol. Crystallogr.*, 1999, **55(10)**, 1718.
35. J. A. Ibers and W. C. Hamilton, *Acta Crystallogr*., 1964, **17(6)**, 781.
36. C. F. Macrae, P. R. Edgington, P. McCabe, E. Pidcock, G. P. Shields, R. Taylor, *et al., J. Appl. Crystallogr*., 2006, **39(3)**, 453.